Research in Astron. Astrophys. **2010** Vol. **10** No. **3**, 199–210
http://www.raa-journal.org *http://www.iop.org/journals/raa*

***R**esearch in*
***A**stronomy and*
***A**strophysics*

The mini-QSO's contribution to cosmic reionization *

Ying-Ying Wang[1], Lei Wang[2], Shou-Ping Xiang[1], Yu Wang[1], Jing-Meng Hao[1] and Ye-Fei Yuan[1]

[1] Center for Astrophysics, University of Science and Technology of China, Hefei 230026, China; *yingying@mail.ustc.edu.cn*
[2] Shanghai Astronomical Observatory, Joint Institute for Galaxy and Cosmology (JOINGC) of SHAO and USTC, Shanghai 200030, China

Received 2009 September 3; accepted 2009 December 23

Abstract By employing an improved simulation of the evolution of black holes (BHs) based on the merger tree of dark matter halos, we explore the relationship between the central BH mass $M_{\rm bh}$ and velocity dispersion σ_* at high redshift $z \geq 6$ and quantify the mini-QSO's (with BH mass $M = 200 - 10^5 M_\odot$) contribution to cosmic reionization. The simulation demonstrates how seed BHs migrate onto the $M_{\rm BH}$-σ_* relation by merging with each other and accreting gas at $z \geq 6$: 1. The correlation between BHs and their host halos increases as the BHs grow; 2. The slope, i.e. $\phi = d\log(M_{\rm bh})/d\log(\sigma_*)$ in the relationship, is insensitive to the redshift at $z > 6$. In agreement with previous work, we find that mini-QSOs' ionizing capability to the Universe lies in the range $\sim 25\% - 50\%$ if early miniquasars have extremely high duty cycles, i.e. $P(z > 6) \sim 0.9 - 1$.

Key words: cosmology: theory — galaxies: evolution

1 INTRODUCTION

Recently, an intermediate-mass BH (IMBH) of over $500\,M_\odot$ was identified in the galaxy ESO 243–49 (Farrell et al. 2009). This finding represents strong evidence for the existence of mini-QSOs. It supports the scenario that seed BHs in mini-QSOs arise from the collapse of massive stellar objects (MSO), i.e. Population III (Pop III) stars which have characteristic masses of $100 - 1000\,M_\odot$.

Study of the highest redshift QSOs implies that the IGM is completely ionized at $z \sim 6$, and consists of less than 50% neutral hydrogen at $z \sim 6.5$ (Fan et al. 2006; Wyithe et al. 2005). The stellar caused reionization has been studied extensively via semi-analytic or/and self-regulated feedback models (Samui et al. 2007; Wang et al. 2008; Wang et al. 2009). Observations of the soft X-ray background (SXRB) put tight constraints on the the density of BHs at high redshift (Dijkstra et al. 2004; Salvaterra et al. 2005). The upper limit of the density of IMBHs at $z \geq 6$ is $\rho_{\rm IMBH} < 3.8 \times 10^4\ M_\odot\ {\rm Mpc}^{-3}$.

Some researchers believe that mini-QSOs caused early relonization. Madau et al. (2004) ran a halo-merger-driven simulation and found that mini-QSOs may be responsible for cosmological reionization at $z \sim 15$. In this paper, we improved this algorithm and considered a more physical

∗ Supported by the National Natural Science Foundation of China.

process, such as a reasonable choice of the seed BHs, consideration of the Eddington ratio λ and the duty cycle of mini-QSOs, P, the improved self-adaptive merger tree model (Yuan et al. 2008), and updated cosmological parameters. Furthermore, we have explored the $M_{\rm bh}$-σ_* relation at high redshift.

This paper is organized as follows. In Section 2, we build the merger tree model for DM halos and test its reliability. Section 3 addresses how the seed BHs are selected in this paper. Section 4 gives a brief description of the $M_{\rm bh}$-σ_* relation and gas accretion onto BHs, and generates the BH merger tree to compare with the $M_{\rm bh}$-σ_* relation. In Section 5, we discuss the mini-QSO's contribution to cosmic reionization. Finally, we summarize our results in the last section. Throughout this paper, we adopt the cosmological parameters consistent with the 5 year WMAP data: $\Omega_{\rm m}h^2 = 0.1369$, $\Omega_\Lambda = 0.721$, $\Omega_{\rm b} = 0.0462$, $h = 0.701$, and $\sigma_8 = 0.817$ (Komatsu et al. 2008).

2 DM HALO MERGER TREE SIMULATION AND ITS TEST

The DM halo merger tree simulation was proposed by Lacey & Cole (1993), and was improved by Somerville & Kolatt (1999), Volonteri et al. (2003) and Yuan et al. (2008). We consider the number of progenitors with mass in the range M to $M+dM$, so the more massive halo of mass M_0 fragments into smaller pieces when one takes a small step δz back in time, which can be expressed as

$$\frac{dN}{dM}(z = z_0) = \frac{1}{\sqrt{2\pi}}\,\frac{M_0}{M}\,\frac{1}{S^{3/2}}\,\frac{d\delta_c}{dz}\,\frac{d\sigma_M^2}{dM}\delta z, \tag{1}$$

where

$$\begin{aligned} \delta_c &= 1.686 \times [1 + 0.012299 \log(1 - \Omega_{\rm m}(z))], \\ \Omega_{\rm m}(z) &= \Omega_{\rm m}(1+z)^3[1 - \Omega_{\rm m} + (1+z)^3\Omega_{\rm m}]^{-1}, \\ S &\equiv \sigma_M^2 - \sigma_{M_0}^2, \end{aligned} \tag{2}$$

and $\sigma(M)$ is the linear theory rms mass fluctuation smoothed with a 'top-hat' filter of mass M. Originally, Volonteri et al. (2003) employed a fixed step method — using 820 timesteps logarithmically spaced in an expansion factor between $z = 0$ and $z = 20$ — and the parameterized fraction of accreted mass [1] to fit the EPS theory. However, Yuan et al. (2008) found that the mean number of fragments N_p exceeds 3 at high redshift, i.e. $z > 15$, which conflicts with the fundamental assumption of binary fragmentation, demanding $N_p \ll 1$. As a solution, they insert a sub-tree in each timestep to ensure that the $N_p > 0.3$ case vanishes. Following Yuan et al. (2008), we develop another self-adaptive step code for the DM halo merger tree. In our algorithm, the timestep δz is determined by the equation

$$N_p = \int_{M_{\rm res}}^{M_{\rm max}/2} \frac{1}{\sqrt{2\pi}}\,\frac{M_{\rm max}}{M}\,\frac{1}{S^{3/2}}\,\frac{d\delta_c}{dz}\,\frac{d\sigma_M^2}{dM}\delta z dM \;=\; 0.2. \tag{3}$$

That means in one generation of halos, even the most massive one (with mass $M_{\rm max}$) can hardly produce multiple fragmentations with such a small mean number of fragments, $N_p = 0.2 \ll 1$. This constraint ensures that other halos of this generation have an $N_p \leq 0.2$. In addition, parameterizing the fraction of accreted mass is no longer necessary for this binary fragmentation mode. Our merger tree has about $5\,000 \sim 15\,000$ timesteps from $z = 0$ to $z = 20$. Thanks to rapidly improved computing technology, these calculations can be finished in a reasonable time. In this paper, we use the modified PS formula proposed by Sheth & Tormen (1999) instead of the original one. The one

[1] After repeating this work (Volonteri et al. 2003), we find a large quantity of multiple fragmentations appear at high redshift; the parameterized fraction of accreted mass (eq. (6) in Volonteri et al. 2003) can give a better fit to the theory prediction than the exact one (eq. (3) in Volonteri et al. 2003). However, multiple fragmentations are inevitable in their work.

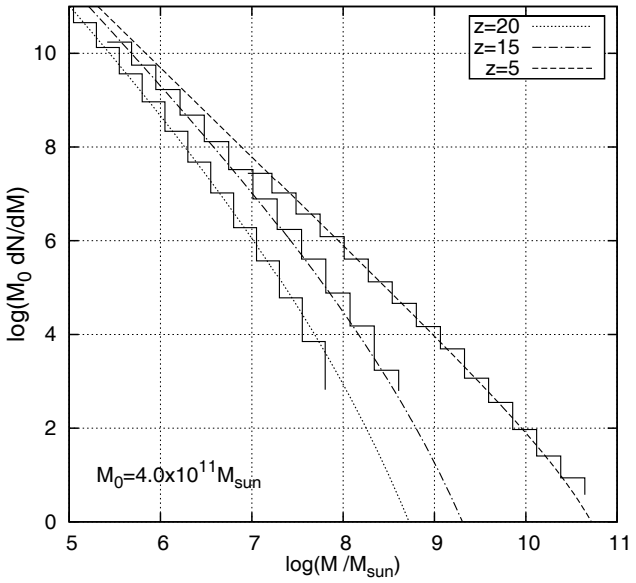

Fig. 1 Mean number density of progenitors with mass M for an $M_0 = M(z = 0) = 4.0 \times 10^{11} M_\odot$ parent halo, at redshifts $z = 5, 15, 20$. *Solid lines*: predictions of the EPS theory. *Histograms:* results for the merger tree (mean of 12 trials), $M > 2 \times M_{\rm res}$.

proposed by Sheth & Tormen (1999) can fit the N-body numerical simulations better, especially at high redshift. The abundance of halos, expressed as the number of halos per unit of comoving volume at redshift z with mass in the interval $(M, M + dM)$, may be written as

$$N_{\rm PS}(M, z)dM = A\left(1 + \frac{1}{\nu'^{2q}}\right)\sqrt{\frac{2}{\pi}}\frac{\rho_{\rm m}}{M}\frac{d\nu'}{dM}\exp\left(-\frac{\nu'^2}{2}\right)dM, \tag{4}$$

where $\nu' = \sqrt{\alpha} \times \delta_c/[D(z)\sigma(M)]$, $A \approx 0.322$, $\alpha = 0.707$ and $q = 0.3$ (Sheth & Tormen 1999; Sheth et al. 2001). Also, $\rho_{\rm m}$ is the current mean density of the universe, and $D(z)$ is the growth factor for linear perturbations,

$$D(z) = \frac{5\Omega_{\rm m}(z)}{2(1+z)}\left[\frac{1}{70} + \frac{209}{140}\Omega_{\rm m}(z) - \frac{\Omega_{\rm m}(z)^2}{140} + \Omega_{\rm m}(z)^{4/7}\right]^{-1}. \tag{5}$$

For a test, we compare our simulation result to the EPS theory predictions of the mean number density of progenitors with mass M at different redshifts in three cases: for parent halos with mass $M_0 = M(z = 0) = 4.0 \times 10^{11}\, M_\odot, 3.7 \times 10^{12}\, M_\odot$ and $4.0 \times 10^{13}\, M_\odot$. Figures 1 and 2 illustrate that in the absence of artificial parameters this algorithm can make the simulation fit the EPS theory predictions very well.

3 SEED BHS AS CENTRAL ENGINES OF THE MINI-QSOS

People usually choose a certain $\nu - \sigma$ peak from the field of cosmological density fluctuations as the lower bound of the mass of halos that contain mini-QSOs (Madau & Rees 2001; Volonteri et al. 2003; Madau et al. 2004). In this scenario, the "container halos" with peaks above

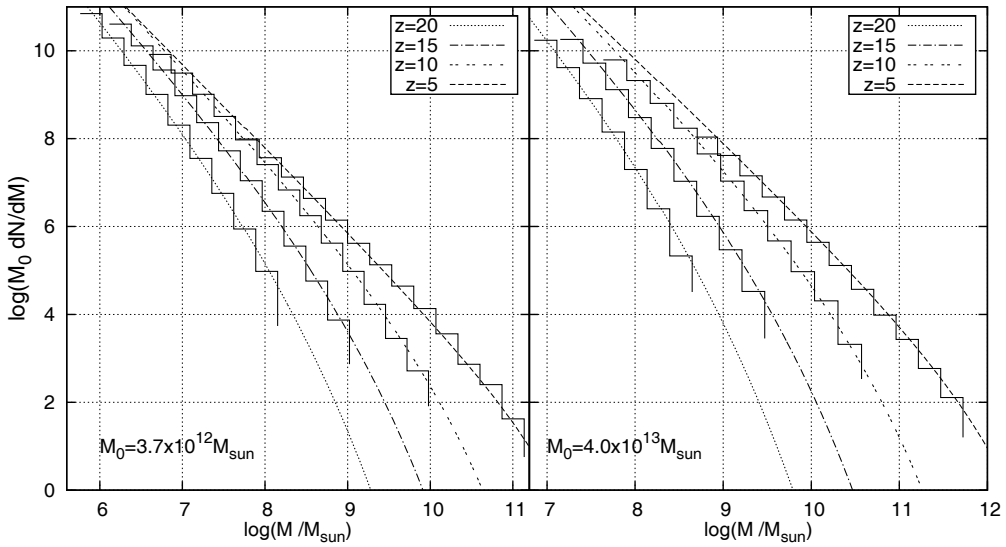

Fig. 2 Same as Fig. 1 for the $M_0 = 3.7 \times 10^{12}$ and $4.0 \times 10^{13} M_\odot$ parent halos. In addition, we insert the $z = 10$ case into the figure.

$3-\sigma$ are considered (corresponding to $1.0 \times 10^7\, M_\odot$). Also, we adopt the BHs derived from Pop III remnants as the initial seeds. It is well-known that the ultimate fate of a Pop III star depends critically on its mass (Heger & Woosley 2002; Heger et al. 2003): $(1)\ 8\, M_\odot < M_* < 25\, M_\odot$: these stars explode as core-collapse SNe and leave neutron stars behind, $(2)\ 25\, M_\odot < M_* < 40\, M_\odot$: these explode as faint Type II SNe and leave black holes behind. $(3)\ 40\, M_\odot < M_* < 140\, M_\odot$: these do not explode as SNe but rather directly collapse into black holes. However, some of them experience a pulsating instability and eject their outer envelope, again leaving behind black holes. $(4)\ 140\, M_\odot < M_* < 260\, M_\odot$: these explode as PISNe, causing complete disruption. (5) $260\, M_\odot < M_*$: these collapse, in the absence of rotation, directly into black holes. We choose the last case, stars with $M_* > 260\, M_\odot$, as the progenitors of the central IMBHs. Since the Pop III stars (i.e. $M_* > 260\, M_\odot$) collapse into BHs with only a small fraction of mass loss (Heger et al. 2003), the seed BHs and their progenitors nearly have the same mass distribution. Here, we employ a slightly top-heavy IMF (Larson 1998) for these seed BHs:

$$\frac{dN_{\rm BH}}{(d\log M_{\rm BH})} \propto (1 + M_{\rm BH}/M_{\rm c})^{-1.35}, \tag{6}$$

where $M_{\rm c} = 100\, M_\odot$ is the characteristic mass of seed BHs.

4 $M_{\rm BH}$-σ_* RELATIONSHIP

It is now widely accepted that the center of most of galaxies harbors a massive black hole. There is a close correlation between the mass of the central galactic black hole $M_{\rm BH}$ and the stellar velocity dispersion σ_*. The $M_{\rm BH}$-σ_* relation has the form below:

$$\log M_{\rm BH} = \theta + \phi \log(\sigma_*/\sigma_0), \tag{7}$$

where $\sigma_0 = 200\,{\rm km\,s^{-1}}$. Tremaine et al. (2002) suggests $\theta = 8.13$ and $\phi = 4.02$ which may express the $M_{\rm BH}$-σ_* relation well at $z \sim 0$. Robertson et al. (2006) proposes that the relationship

with parameters $\theta = 7.44$ and $\phi = 3.62$ agrees with the $z \sim 6$ case. Which values will be assigned to these parameters for mini-QSOs at $z > 6$? This is the goal of this paper. The stellar velocity dispersion σ_* is linked to the circular velocity of halos, V_c, by the relationship (Ferrarese 2002; Pizzella et al. 2005):

$$\log V_c = 0.84 \log \sigma_* + 0.55. \tag{8}$$

Following Barkana & Loeb (2001), the circular velocity V_c is a function of halo mass M and redshift z, which reads:

$$V_{\rm c} = 23.4 \left(\frac{M}{10^8 h^{-1} M_\odot}\right)^{1/3} \left[\frac{\Omega_{\rm m}}{\Omega_{\rm m}^z} \frac{\Delta_{\rm c}}{18\pi^2}\right]^{1/6} \left(\frac{1+z}{10}\right)^{1/2} {\rm km\ s^{-1}} \tag{9}$$

with

$$\Delta_{\rm c} = 18\pi^2 + 82d - 39d^2 \tag{10}$$

and $d \equiv \Omega_{\rm m}(z) - 1$. Now, Equations (7), (8) and (9) closely associate the IMBH mass $M_{\rm BH}$ with halo mass M and redshift z.

4.1 Gas Accretion onto BHs

To start the simulation, each "container halo" is randomly assigned a central BH [2]. The masses of these seed BHs are distributed as shown in Equation (6), in the mass range $200 M_\odot < M_{\rm BH} < 1000\, M_\odot$ [3]. The growth of a central BH depends on both gas accretion and progenitor BHs mergers. Gas accretion onto BHs leads to miniquasars shining and the mass density of their associated BHs increasing. However, the BHs' meger does not result in the growth of mass density of BHs. For an active BH of mass $M_{\rm BH}$, its growth rate of mass due to gas accretion is then $\dot{M}_{\rm BH} = M_{\rm BH}/t_{\rm ef}$, where the e-folding time is (Salpeter 1964)

$$t_{\rm ef} \ = \ 4 \times 10^7 \left[\frac{\epsilon}{0.1} \frac{1}{\lambda(1-\epsilon)}\right] {\rm yr}, \tag{11}$$

where ϵ is the radiative efficiency (or the mass-to-energy conversion efficiency), and λ is the Eddington ratio. As suggested by Shankar et al. (2008, 2009), a fixed value of $\lambda = 0.25$ is used throughout this paper. At the same time, the mass-to-energy conversion efficiency ϵ varies within a broad range of 0.06–0.3 (depending on the BH's spin). When the magnetohydrodynamic (MHD) effect is considered, the upper limit of a BH's spin decreases from $\hat{a} \simeq 0.995$ (Shakura-Sunyaev disk model, SSD) to $\hat{a} \simeq 0.95$, resulting in a low mass-to-energy conversion efficiency $\epsilon \leq 0.25$, which is especially low at high redshift (Yuan et al. 2008). Here, we cite $\epsilon = 0.075$ (Shankar et al. 2008) and 0.16 (Yu & Lu 2008) as our reference values.

The time duration of the BH growth due to gas accretion (or the time interval in which the BH appeared as a QSO), the so-called lifetime of a QSO $\tau_{\rm lf}$, is currently uncertain but is constrained to lie in the range of 10^6–10^8 yr (Martini 2004). $\tau_{\rm lf} \leq 10^7$ yr is favored by the current result from 2dF (Croom et al. 2004). However, Yu & Tremaine (2002) estimate that the mean lifetime of luminous quasars is $(3-13) \times 10^7$ yr. Here, we employ a parameter called 'duty-cycle' P - the probability that a BH is in the active state - to describe the duration of the accretion process. Wang et al. (2006) found that P has a strong evolution which follows the history of the cosmic star formation rate density in the Universe. Shankar et al. (2008) suggested that the high redshift mini-QSOs should have higher duty cycles, e.g. $P \sim 0.2, 0.5$, and 0.9 at $z = 3.1, 4.5$ and 6, respectively. In this

[2] note that the mass correlation between the 'seed' BH and its "container halo" is unknown at present.

[3] here the small fraction of mass loss is taken into account.

work, we formulate this evolution with $P(z) = 0.03 + 0.97(z/z_{\rm tran})^{\beta}/[1 + (z/z_{\rm tran})^{\beta}]$, in which β is a free parameter describing the transition speed. $P(z)$ with $\beta = 2$ and $z_{\rm tran} = 4$ can provide a good match to the results mentioned above. Then, the mean growth rate due to gas accretion is $\langle \dot{M}_{\rm BH} \rangle = P(z) M_{\rm BH}/t_{\rm ef}$.

4.2 BH Merging Tree

Following Volonteri et al. (2003) and Yuan et al. (2008), we take the BH binary evolution and triple BH interaction into account to generate the BH merger tree. In fact, one can check whether the final BH mass agrees with the present $M_{\rm BH}$-σ_* relation in its host halo (i.e. the parent halo). Figure 3 illustrates how the radiative efficiency ϵ affects the final BH mass in the simulation. What the different symbols represent are marked on the figure [4]. The dotted line represents the present $M_{\rm BH}$-σ_* relation with $\theta = 8.13$ and $\phi = 4.02$ (Tremaine et al. 2002). Obviously, simulations with $\epsilon = 0.16$ (and $\lambda = 0.25$) agree with the currently accepted $M_{\rm BH}$-σ_* relation better than those with $\epsilon = 0.075$ (and $\lambda = 0.25$). Moreover, the later ones lead to an overestimation of the mass density of IMBHs at high redshift. This issue will be discussed soon.

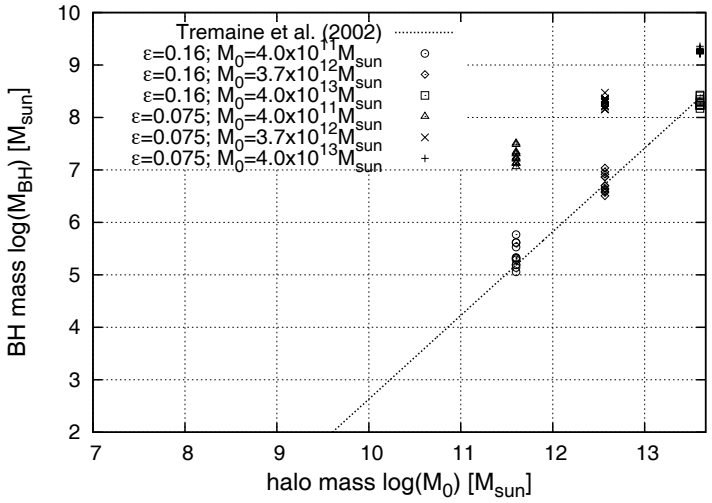

Fig. 3 How the radiative efficiency ϵ affects the final BH mass in the simulation. Here is a figure about the halo mass M_0 vs. its central BH mass $M_{\rm BH}$. What the different symbols stand for are marked on the figure (we do 12 trials for each case). The dotted line represents the present $M_{\rm BH}$-σ_* relation with $\theta = 8.13$ and $\phi = 4.02$ (Tremaine et al. 2002).

By using the simulations with $\epsilon = 0.16$ and $\lambda = 0.25$, one can fit the $M_{\rm BH}$-σ_* relation for $z > 6$. Figures 4, 5 and 6 show how the central BH evolves in its host halo for the parent halo mass $M_0 = 4.0 \times 10^{11}\, M_{\odot}, 3.7 \times 10^{12}\, M_{\odot}$ and $4.0 \times 10^{13}\, M_{\odot}$ (the diamonds, with a total of 12 trials). Here, the dotted and dashed lines represent the $M_{\rm BH}$-σ_* relation with parameters $\theta = 8.13$ and $\phi = 4.02$ (Tremaine et al. 2002) and $\theta = 7.44$ and $\phi = 3.62$ (Robertson et al. 2006) respectively [5]. The bold line with $\theta = 6.67$ and $\phi = 2.79$ is able to provide a good fit to the simulation data in this work for $z > 6$.

[4] We do 12 trials for each case, corresponding to 12 units for each kind of symbols.

[5] Eq. (8) is included to translate the halo's velocity dispersion σ_* into its mass M.

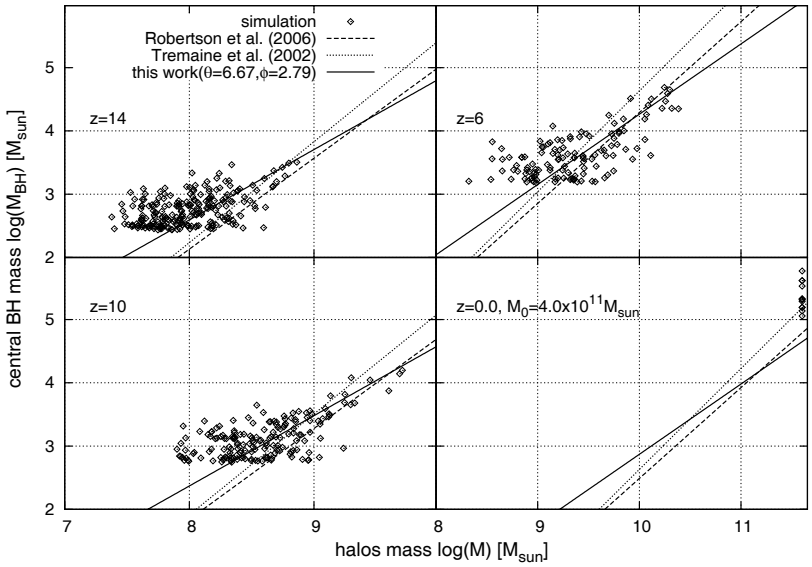

Fig. 4 Halo mass M vs. its central BH mass $M_{\rm BH}$ (the diamonds, simulations with $\epsilon = 0.16$ and $\lambda = 0.25$, with a total of 12 trials) as different redshifts for the parent halo $M_0 = 4.0 \times 10^{11} M_\odot$. The dotted and dashed lines represent the $M_{\rm BH}$-σ_* relation with parameters $\theta = 8.13$ and $\phi = 4.02$ and $\theta = 7.44$ and $\phi = 3.62$ respectively. The bold one stands for the new choice of parameters $\theta = 6.67$ and $\phi = 2.79$ in this work.

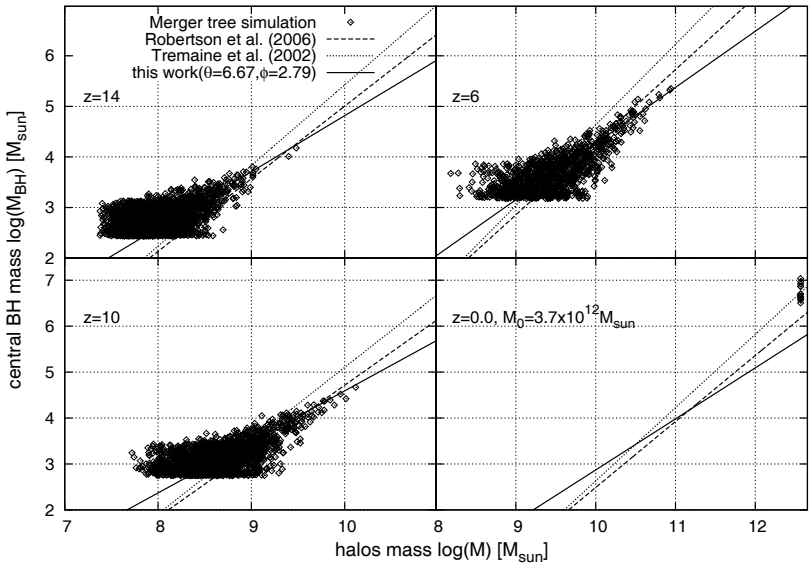

Fig. 5 Same as Fig. 4 for $3.7 \times 10^{12} M_\odot$ parent halo.

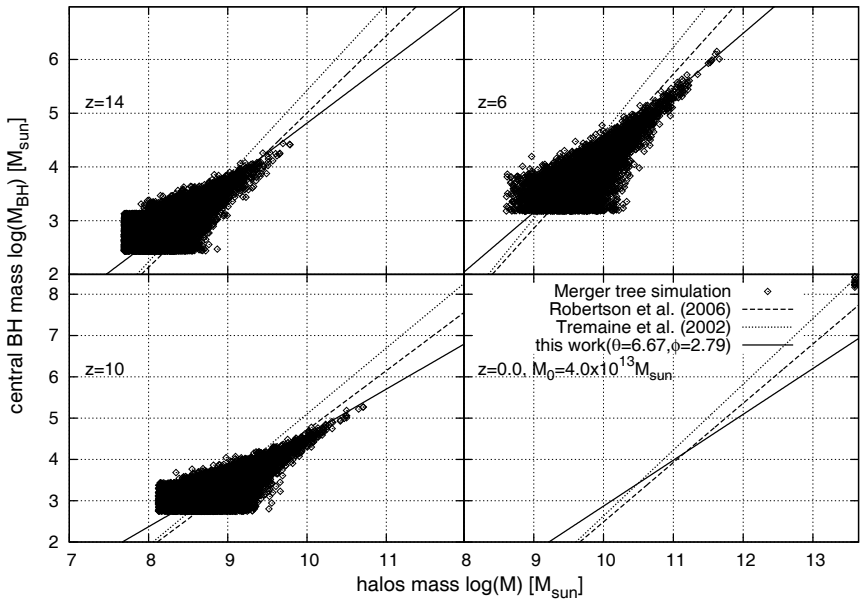

Fig. 6 Same as Fig. 4 for $4.0 \times 10^{13} M_{\odot}$ parent halo.

Figures 4, 5 and 6 illustrate: 1. In the logarithmic coordinate system, the slope ϕ is insensitive to the redshift at $z > 6$, but very sensitive to z at low redshift ($\phi(z = 6) = 2.79$ to $\phi(z \sim 0) = 4.02$). So, one pair of values for θ and ϕ, i.e. $(6.67, 2.79)$, can match the simulation well at different redshifts ($z \geq 6$). 2. Massive parent halo has more 'container halos,' and more BH mergers than the light one at high redshift. 3. Correlation between massive BHs and their host halos is stronger than that between IMBHs and their 'container halos.'

4.3 Soft X-ray Background (SXRB) and the Mass Density of BHs

Mini-QSOs forming at $z > 6$ can contribute to the SXRB. Dijkstra et al.(2004) show that a population dominated by mini-QSOs could still partially ionize the IGM at $z > 6$, but its contribution would be severely constrained if the X-ray background is further resolved into discrete sources. By observing the current SXRB and removing the resolved fraction of the SXRB, Salvaterra et al. (2005) derived the density of IMBHs (active or not) at $z > 6$ of $\rho_{\rm IMBH} < 3.8 \times 10^4\ M_{\odot}$ Mpc^{-3}, about $\simeq 10\%$ of the present day SMBH mass density (Yu & Tremaine 2002).

By using the $M_{\rm BH}$-σ_* relation with new parameters $\theta = 6.67$ and $\phi = 2.79$ and the PS formula (Eq.4), one can compute the BH mass density as a function of redshift. Figure 7 illustrates how the mass density of IMBHs and MBHs varies with redshift. As a reference, we also plot the curves for $\epsilon = 0.075$ (with fitting parameters $\theta = 7.93$ and $\phi = 3.02$) in this figure. The long-dashed line is the upper limit of the density of IMBHs at $z > 6$, $3.8 \times 10^4\, M_{\odot}$ Mpc^{-3}. We are interested in the mass of IMBHs with $200\, M_{\odot} < M_{\rm BH} < 10^5\, M_{\odot}$; the bold line ($\epsilon = 0.16$) and the dot-dashed line ($\epsilon = 0.075$). The short-dashed and dotted lines represent the density of massive BHs for different ϵ values respectively. The low radiative efficiency case ($\theta = 7.93$ and $\phi = 3.02$) overestimates the mass density of the IMBHs, and fails to meet the constraint from the SXRB. In addition, the case with $\theta = 6.67$ and $\phi = 2.79$ agrees with the constraint well at $z > 6$. We also notice that in the later

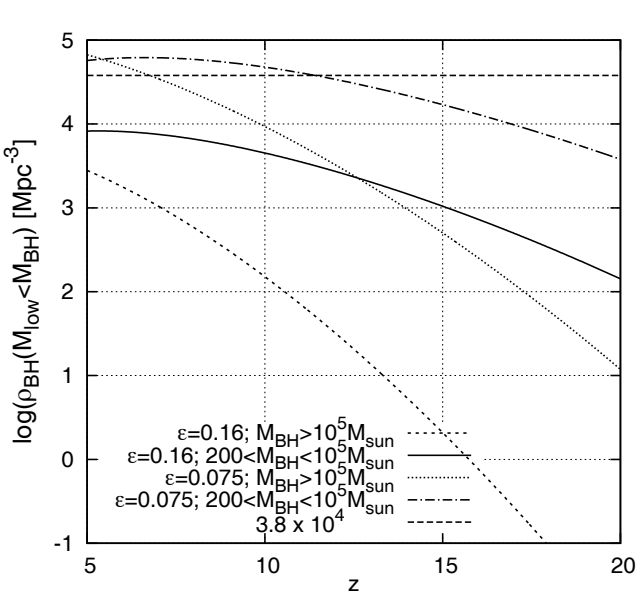

Fig. 7 BH mass density as a function of redshift. The dashed line is the constraint from SXRB. The bold line ($\epsilon = 0.16$) and the dash-dotted one ($\epsilon = 0.075$) stand for the mass density of the IMBH with mass $200M_\odot < M_{\rm BH} < 10^5 M_\odot$. The short-dashed line and dotted one represent that of the massive BHs.

case, most of the mass is absorbed by the IMBHs at an early epoch, instead of the massive or super massive BHs. Moreover, the change of ϵ affects the massive BHs more than it does to the IMBHs.

5 EARLY REIONIZATION BY MINIQUASARS

During the time that a mini-QSO is active, the high flux of X-ray emission can ionize the surrounding medium, e.g. the neutral hydrogen (HI), helium (HeI) or the primarily ionized helium (HeII). Eventually, an ionized zone forms within a sphere (the so-called Stromgren sphere). Following Shapiro & Giroux (1987), in one unit volume of an expanding and evolving HII region, the ionized volume $V_{\rm ion}$ is given by (with the ionized H recombinations and cosmological expansion considered)

$$\bar{n}_{\rm H}^0 \frac{dV_{\rm ion}}{dt} = \frac{dN_\gamma}{dt} - \alpha_{\rm B}(\bar{n}_{\rm H}^0)^2(1+z)^3 \times C \times V_{\rm ion}, \tag{12}$$

where $n_{\rm H}^0$ is the present number density of hydrogen, $\alpha_{\rm B} \simeq 2.6 \times 10^{-13}$ cm^3 s^{-1} is the case B recombination coefficient at $T \simeq 10^4$ K (Seager et al. 1999; Barkana & Loeb 2001), and the volume-averaged clumping factor of the IGM, C, defined as $C \equiv \langle n_{\rm H}^2 \rangle / [(1+z)^3 \bar{n}_{\rm H}^0]^2$. We have assumed the following simple form for C, given by Haiman & Bryan (2006): $C(z) = 1 + 9[7/(1+z)]^2$ for $z \geq 6$ and $C(z) = 10$ for $z < 6$. Also, dN_γ/dt is the rate of UV photons radiated by the mini-QSO in a unit volume, which is determined by a set of quantities:

1. Mass density of IMBHs;

2. The Eddington ratio, λ;

3. The fraction of UV photons which escape from the IMBH host halo, $f_{\rm esc}$, here adopting the same one as for Pop III stars [6], $f_{\rm esc} = 0.8$ (Wang et al. 2009);

[6] Since the IMBHs and Pop III stars are nearly in the same environment.

4. One of the biggest uncertainties in discussing reionization by mini-QSOs, their unknown emission spectrum. A general solution is to use a "multicolor disk blackbody" component plus a simple power-law component to fit the mini-QSO's spectrum (Mitsuda et al. 1984; Tanaka & Levin 1995; Dijkstra et al. 2004; Salvaterra et al. 2005). Here, we keep the forms of the former three factors that have been mentioned in Section 4 intact. It is convenient to assume that a fraction $f_{\rm UV}$ of the bolometric power radiated by the IMBH driven mini-QSOs is emitted as ionizing photons with mean energy $\langle h\nu\rangle$. Moreover, $f_{\rm UV}/\langle h\nu\rangle \times L$ yields the number of ionizing photons for a given spectral emission (Madau et al. 2004). For the mini-QSO's power-law component, $f_{\rm UV}/\langle h\nu\rangle$ is about $0.2\ {\rm ryd}^{-1}$ [7]; for normal quasars, $f_{\rm UV}/\langle h\nu\rangle = 0.1\ {\rm ryd}^{-1}$. In fact, the existence of the "multicolor disk black body" component makes the total spectrum of a mini-QSO be softer than its power-law component, thus resulting in the $f_{\rm UV}/\langle h\nu\rangle$ being less than $0.2\ {\rm ryd}^{-1}$. In this paper, we take $f_{\rm UV}/\langle h\nu\rangle = \ 0.1, 0.15$ and 0.2 as our reference values. Now, dN_γ/dt can be evaluated by

$$\frac{dN_\gamma}{dt} = f_{\rm esc}\frac{f_{\rm UV}}{\langle h\nu\rangle}\lambda\bar{L}\,, \tag{13}$$

$$\begin{aligned}\bar{L} &= \int_{200M_\odot}^{10^5 M_\odot} N_{\rm PS}(M(M_{\rm BH},z),z)L_{\rm Edd}(M_{\rm BH})dM_{\rm BH} \\ &= 1.26\times10^{38}\frac{\rho_{\rm IMBH}(z)}{M_\odot}\ {\rm erg\ s^{-1}\ Mpc^{-3}}\,,\end{aligned} \tag{14}$$

$$L_{\rm Edd}(M_{\rm BH}) = 1.26\times10^{38}\frac{M_{\rm BH}}{M_\odot}\ {\rm erg\ s^{-1}},$$

where $\bar{L}$ is the volume averaged luminosity, the total luminosity radiated by mini-QSOs per unit of comoving volume.

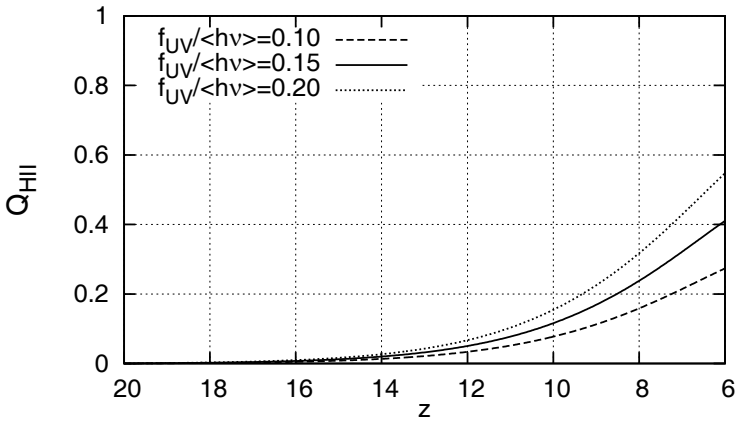

Fig. 8 Mini-QSOs reionization history for different cases. *Dashed line*: $f_{\rm UV}/\langle h\nu\rangle = 0.1$; *bold line*: $f_{\rm UV}/\langle h\nu\rangle = 0.15$; *dotted line*: $f_{\rm UV}/\langle h\nu\rangle = 0.2$.

Figure 8 shows how the spectral parameter $f_{\rm UV}/\langle h\nu\rangle$ affects the reionization history. If the mini-QSO has a normal QSO-like spectrum, their reionizing contribution to the Universe is not

[7] $L_\nu \propto \nu^{-1}$ and $13.6\ {\rm eV} \le h\nu \le 2\ {\rm keV}$.

very significant, $\sim 25\%$ at $z \sim 6$. This basically agrees with Madau et al. (2004) and Ricotti & Ostriker (2004) in that mini-QSOs with mass $10^2 M_\odot \leq M_{\rm BH} \leq 10^5 M_\odot$ can lead to a low level $10\% - 30\%$ partial ionization in the low density IGM. In contrast, it can nearly dominate the cosmological reionization if the mini-QSOs radiate all their energy in a hard power-law spectrum, i.e. $f_{\rm UV}/\langle h\nu \rangle = 0.2$. In the absence of further constraints on the spectral parameters, in the intermediate case - $f_{\rm UV}/\langle h\nu \rangle = 0.15$, about 40% of the IGM ionized at $z \sim 6$ - is a fair choice, which agrees with the previous work: 'Distant miniquasars that produce enough X-rays to only partially ionize the IGM to a level of at most 50% (Dijkstra et al. 2004).' Note that these results are based on the premise that mini-QSOs hardly quench at high redshift, i.e. $P(z > 6) \sim 0.9 - 1$. If they have a duty cycle like that of present QSOs $P(z \sim 0) \sim 0.1$, their contribution to the reionization would be negligible.

6 DISCUSSIONS AND CONCLUSIONS

In this paper, we discuss the ionizing contribution of those early mini-QSOs ($z \geq 6$) within the framework of the Lambda Cold Dark Matter (LCDM) model. By using a Monte-Carlo method based DM halo merger tree simulation, we fit the $M_{\rm bh}$-σ_* relation at high redshift and adopt this relation in the subsequent computation with the parameterized UV photon emission efficiency of mini-QSOs. However, this paper undergoes some arguments or uncertainties due to model simplification or parametrization as follows. (i). In order to understand the ionizing effect from the mini-QSOs, we neglect the contributions from stars. The first stars in a star forming halo usually ionize their surrounding IGM before the mini-QSO appears. In practice, the two objects can affect each other via radiative feedback mechanisms [8]. However, the additional complexity goes beyond the scope of this paper. It is certain that we will consider this point in future work. (ii). Actually, in Section 4 one can obtain the same fitting parameters (θ, ϕ) by varying λ and ϵ simultaneously to keep the e-folding time unchanged. However, lacking direct observations and a convictive theory (or simulations) of the high-redshift mini-QSO, a parametrization can help us paint a general picture about this quasar population. The upcoming launch of the *James Webb Space Telescope* (JWST), the successor of the *Hubble Space Telescope* (HST) (Barkana & Loeb 2001), is expected to find the Pair Instability SNe that indicates the existence of massive Pop III stars (Wise & Abel 2005). The Lyα spheres generated by the first luminous objects will be directly detected by the next generation 21 cm instruments. Also, detecting these regions of Lyα absorption can help us understand the properties of the first luminous objects, such as their mass distribution and spatial correlation (Chen & Miralda-Escude 2008).

Generally, our simulation shows how the seed BHs migrate onto the $M_{\rm BH}$-σ_* relation by merging with each other and accreting gas at $z \geq 6$. In addition, the correlation between BHs and their host halos increases as the BHs grow. Simulation with low radiative efficiency, e.g. $\epsilon = 0.075$, cannot agree with the present observed $M_{\rm BH}$-σ_* relation, which leads to an overestimation of the mass density of IMBHs and the SXRB at high redshift. The slope ϕ in the relationship is insensitive to the redshift at $z > 6$. So, one pair of values for θ and ϕ, i.e. (6.67,2.79), can match the simulation well at different redshifts ($z \geq 6$).

Further calculation shows the mini-QSOs' ionizing capability in the Universe lies in the range $\sim 25\% - 50\%$ if miniquasars can be well fed and then have high duty cycles, i.e. $P(z > 6) \sim 0.9 - 1$ at an early epoch.

Acknowledgements We thank the anonymous referee for helpful comments that improved the presentation of this paper. This work is partially supported by the National Basic Research Program of China (2009CB824800), the National Natural Science Foundation of China (Grant Nos. 10733010, 10673010 and 10573016), and the Program for New Century Excellent Talents in University.

[8] The stars' feedback mechanisms are extensively investigated by Wang et al. (2009).

References

Barkana, R., & Loeb, A. 2001, Phys. Rep., 349, 125
Chen, X., & Miralda-Escude, J. 2008, ApJ, 684, 18
Croom, S., et al. 2004, in ASP Conf. Ser. 311, AGN Physics with the Sloan Digital Sky Survey, eds. G. T. Richards, & P. B. Hall (San Francisco, CA: ASP), 457
Dijkstra, M., Haiman, Z., & Loeb, A. 2004, ApJ, 613, 646
Fan, X., Strauss, M. A., Richards, G. T., et al. 2006, AJ, 131, 1203
Farrell, S. A., Webb, N. A., Barret, D., Godet, O., & Rodrigues, J. M. 2009, Nature, 460, 73
Ferrarese, L. 2002, ApJ, 578, 90
Haiman, Z., & Bryan, G. 2006, ApJ, 650, 7
Heger, A., & Woosley, S. E. 2002, ApJ, 567, 532
Heger, A., Fryer, C. L., Woosley, S. E., Langer, N., & Hartmann, D. H. 2003, ApJ, 591, 288
Komatsu, E., Dunkley, J., et al. 2009, ApJS, 180, 330
Lacey, C., & Cole, S. 1993, MNRAS, 262, 627
Larson, R. B. 1998, MNRAS, 301, 569
Madau, P., & Rees, M. J. 2001, ApJ, 551, L27
Madau, P., Rees, M. J., Volonteri, M., Haardt, F., & Oh, S. P. 2004, ApJ, 604, 484
Martini, P. 2004, Coevolution of Black Holes and Galaxies, ed. L. C. Ho (Cambridge: Cambridge University Press), 169
Mitsuda, K., et al. 1984, PASJ, 36, 741
Pizzella, A., et al. 2005, ApJ, 631, 785
Ricotti, M., & Ostriker, J. P. 2004, MNRAS, 352, 547
Robertson, B., et al. 2006, ApJ, 641, 90
Salpeter, E. E. 1964, ApJ, 140, 796
Salvaterra, R., Haardt, F., & Ferrara, A. 2005, MNRAS, 362, L50
Samui, S., Srianand, R., & Subramanian, K. 2007, MNRAS, 377, 285
Shankar, F., Crocce, M., Miralda-Escude, J., Fosalba, P., & Weinberg, D. H. 2008, arXiv: 0810.4919
Shankar, F., Weinberg, D. H., & Miralda-Escude, J. 2009, ApJ, 690, 20
Shapiro, P. R., & Giroux, M. L. 1987, ApJ, 321, L107
Sheth, R. K., Mo, H. J., & Tormen, G. 2001, MNRAS, 323, 1
Sheth, R. K., & Tormen, G. 1999, MNRAS, 308, 119
Seager, S., Sasselov, D. D., & Scott, D. 1999, ApJ, 523, L1
Somerville, R. S., & Kolatt, T. S. 1999, MNRAS, 305, 1
Tanaka, Y., Lewin, W. H. G. 1995, X-Ray Binaries, eds. W. H. G. Lewin, J. van Paradijs, & E. P. J. van den Heuvel (Cambridge: Cambridge Univ. Press), 126
Tremaine, S., et al. 2002, ApJ, 574, 740
Volonteri, M., Haardt, F., & Madau, P. 2003, ApJ, 582, 559
Wang, J., Chen, Y., & Zhang, F. 2006, ApJ, 647, L17
Wang, L., Mao, J., Xiang, S., & Yuan, Y. 2008, ChJAA (Chin. J. Astron. Astrophys.), 8, 631
Wang, L., Mao, J., Xiang, S., & Yuan, Y. 2009, A&A, 2009, 494, 817
Wise, J. H., & Abel, T. 2005, ApJ, 629, 615
Wyithe, J. S. B., Loeb, A., & Carilli, C. 2005, ApJ, 628, 575
Yu, Q., & Lu, Y. 2008, ApJ, 689, 732
Yu, Q., & Tremaine, S. 2002, MNRAS, 335, 965
Yuan, Y. F., Zhang, C. Y., Yang, J. M., Wang, L., Lin, X. B., Xu, S. N., & Zhang, J. L. 2008, AIPC, 968, 369